Quasiperiodic Raman Technique for Ultrashort Pulse Generation

D. D. Yavuz, D. R. Walker, M. Y. Shverdin, G. Y. Yin, and S. E. Harris

Edward L. Ginzton Laboratory, Stanford University, Stanford, California 94305, USA

We report the experimental demonstration of a new Raman technique that produces 200 sidebands, ranging in wavelength from 3 μm to 195 nm. By studying multiphoton ionization of nitric oxide (NO) molecules, we show mutual phase coherence among 15 visible sidebands covering 0.63 octaves of bandwidth.

A new approach for generating ultrashort pulses of radiation utilizes coherently oscillating molecules [1,2]. Two laser fields, whose frequency difference is slightly detuned from a Raman resonance, will prepare the molecules in a superposition of states $|g\rangle$ and $|e\rangle$ (Fig. 1). When the intensities of the two driving lasers are sufficiently large, the magnitude of the coherence of the Raman transition approaches its maximum value, $|\rho_{ge}| = 0.5$. Such a coherently vibrating ensemble of molecules acts as a local oscillator and modulates the driving lasers, producing collinear sidebands spanning over four octaves of bandwidth. Recent experiments have demonstrated the generation of vibrational and rotational Raman spectra covering the infrared, visible, and ultraviolet spectral regions in molecular deuterium (D_2), hydrogen (H_2), and solid H_2. Sokolov and colleagues have shown phase coherence among five vibrational Raman sidebands and demonstrated the generation of a near-single-cycle pulse structure [3]. Two limitations of this Raman technique are (i) the generated number of sidebands is low, limiting the number of terms of the Fourier series available for temporal pulse shaping, and (ii) the synthesized time waveform is a periodic train of pulses with a pulse spacing which is determined by the Raman transition frequency. As an example, in D_2, the $\nu'' = 0 \rightarrow \nu' = 1$ vibrational transition is 2994 cm^{-1} and the time between pulses is 11 fs.

In this Letter we demonstrate a quasiperiodic Raman technique that overcomes these limitations [4]. Noting Fig. 1, we drive two Raman resonances with different oscillation frequencies and produce 200 sidebands with frequencies of the form

$$\omega_{q,r} = \omega_0 + q\omega_a + r\omega_b, \tag{1}$$

where q and r are integers and ω_a and ω_b are the frequencies of the respective Raman transitions. We demonstrate phase coherence among 15 sidebands by studying multiphoton ionization of nitric oxide (NO) molecules. In general, the ratio of the two transition frequencies, ω_a/ω_b, is irrational. As a result, the double Fourier series of Eq. (1) synthesizes a quasiperiodic time waveform $E(t)$. Formally, quasiperiodicity means that, for every $\epsilon > 0$, there exists a τ_ϵ such that [5]

$$|E(t) - E(t - \tau_\epsilon)| < \epsilon, \tag{2}$$

for all t. The key advantage of the quasiperiodic technique is that the number of sidebands that is produced is equal to the product of the number of sidebands generated by each Raman excitation alone. If the respective cells produce N_a and N_b sidebands, then the two cells in series produce a total of $N_a N_b$ sidebands with a bandwidth of $N_a \omega_a + N_b \omega_b$. By adjusting the phases of the respective Fourier components of this spectrum, we may obtain a waveform with a prescribed temporal shape. This waveform is quasiperiodic; i.e., at seemingly random times, the prescribed pulse comes close to replicating itself. These replications occur with an average periodicity of [4]

$$T = (2\pi)\frac{N_a N_b}{N_a \omega_a + N_b \omega_b}. \tag{3}$$

This average periodicity may be made quite large. For example, if $\omega_a \approx \omega_b$ and $N_a \approx N_b$, $T \approx \pi N_a/\omega_a$. For $N_a = N_b = 30$ and $\omega_a \approx \omega_b = 500$ cm^{-1}, the average periodicity is 1 ps. Mode locking such a spectrum would produce pulses with a maximum peak power enhancement of about 900. This waveform will have pulses within 80% of maximum enhancement on average once every several picoseconds with smaller amplitude pulses occurring more frequently.

We cite related earlier work: The idea of using a Raman spectrum for synthesizing ultrashort pulses was
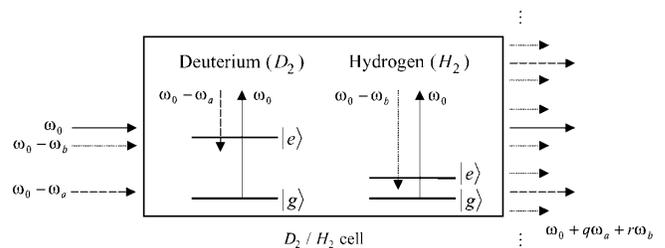
FIG. 1. Schematic of successive molecular modulators. A pair of lasers drives coherent vibrations in molecular D_2, whereas another pair drives coherent rotations in H_2. The frequency difference of the driving lasers is slightly detuned from the Raman resonance so as to adiabatically prepare the molecules in a superposition state.

originally suggested by Yoshikawa and Imasaka and by Kaplan and co-workers [6,7]. Nazarkin and colleagues have demonstrated the generation of $\approx$ 4-fs-wide pulses by using impulsive excitation of various molecules [8]. Losev and co-workers and Kawano and co-workers have demonstrated efficient Raman generation by using two-color excitations [9,10]. Uetake and co-workers have demonstrated the generation of a broad rovibrational spectrum in a liquid hydrogen droplet [11]. Bartels *et al.* have shown phase modulation of ultrashort pulses by reviving rotational wave packets [12]. Researchers in the field of high-harmonic generation have recently achieved generation of subfemtosecond pulses in the soft x-ray region of the spectrum [13]. The most common technique for generating ultrashort pulses ($\approx$ 4 fs) in the visible region relies on broadening the spectrum of a Ti:sapphire laser [14]. Ultrashort pulses are now used to coherently control many molecular and chemical processes [15–17].

We proceed with the description of our experiment. We use a Nd:YAG and two Ti:sapphire lasers to drive the $\nu'' = 0, J'' = 0 \rightarrow \nu' = 1, J' = 0$ vibrational transition in D_2 at 2994 cm^{-1}, and $\nu'' = 0, J'' = 1 \rightarrow \nu' = 0, J' = 3$ rotational transition in H_2 at 587 cm^{-1}. The Nd:YAG laser is a commercial Spectra Physics Quanta Ray laser at 1.06 μm. The Ti:sapphire lasers are custom-made laser systems pumped by the second harmonic of separate Nd:YAG Spectra Physics Quanta Ray lasers. These lasers are injection seeded by laser diodes and produce transform-limited 15-ns-long, 60-mJ pulses at the seeding wavelength. The seeding wavelengths of the diode lasers are tunable and monitored with a wave meter. The three laser beams are focused to a spot size of about 500 μm in the D_2/H_2 cell. The intensity of each laser at the focus is about 2 GW/cm^2, and both Raman transitions are driven about 300 MHz below resonance, allowing us to adiabatically prepare a coherence of peak magnitude $|\rho_{ge}| \approx 0.2$ (see Ref. [18]) for each molecular species. Our Raman cell is cooled to a temperature of 77 K with liquid N_2. Cooling increases the population of the rotational levels that we access and also reduces the Doppler linewidth. The D_2 pressure is 60 torr and the H_2 pressure is 30 torr. These pressure values are 2 to 3 orders of magnitude lower than those used in traditional Raman scattering experiments.

At the output of the Raman cell we see a bright white beam. The generated spectrum, after dispersion with a prism, is shown in Fig. 2. A rovibrational spectrum ($q = -3, -2, \ldots, 13$; $r = -5, -4, \ldots, 6$) with approximately 200 Raman sidebands ranging in wavelength from 1.06 μm to 195 nm is produced [Fig. 2(a)]. To our knowledge, this is the largest number of sidebands ever generated in a Raman scattering experiment. Figure 2(b) is an expansion of the visible portion of the spectrum of Fig. 2(a). Interleaving sidebands are produced when the width of the generated rotational spectrum exceeds the vibrational spacing. By using additional dispersion on the vibrational violet sideband, we can resolve two of these neighboring rovibrational sidebands [Fig. 2(c)]. With phase control, the spectrum of Fig. 2(a) should ultimately allow the generation of high-peak-power, subfemtosecond pulses, separated, on average, by $T \approx 0.15$ ps.

We now proceed with the description of correlation studies of the temporal waveform. The spectrum is dispersed with a pair of SF10 glass prisms after the Raman cell (Fig. 3). The distance between these prisms is selected such that 15 sidebands enter the second prism and then go through the programmable liquid-crystal, spatial-light modulator. The liquid-crystal modulator is manufactured by Jenoptik Jena and consists of a linear array of 640 pixels. The width of each pixel is 97 μm, and there is a 3 μm gap between adjacent pixels. The refractive index of each pixel can be electronically controlled by applying a (computer-controlled) specified voltage. This enables us to independently adjust the phase of each sideband. Because the liquid crystal operates from 1.5 μm to 420 nm and, to avoid damage from the energetic, near-infrared driving lasers, we select 15 visible sidebands for phase control. These sidebands extend from 650 nm ($q = 1$, $r = 0$) to 420 nm ($q = 4$, $r = -1$) in wavelength. Since the dispersion setup cannot sufficiently separate interleaving sidebands, we are limited to using $r = -2$, $-1, 0, 1, 2$. After phase adjustment, the sidebands are spatially recombined with another prism pair and focused into an NO ionization chamber. The alignment of the prism setup is achieved by imaging the focal spot with a microscope objective. The NO pressure is $\approx 10^{-5}$ torr,
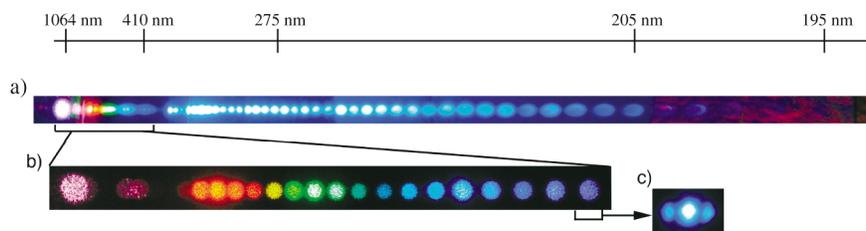
FIG. 2 (color).   The combined rovibrational spectrum: (a) 200 sidebands are generated ranging in wavelength from 1.06 μm to 195 nm. The spectrum extends to 3 μm in the infrared [not captured by the charge-coupled device (CCD) camera]. Certain parts of the spectrum are attenuated by neutral density filters to reduce CCD camera saturation. (b) Expansion of the visible portion of the spectrum of part (a). (c) Further dispersion of the vibrational violet sideband shows two interleaving sidebands that result from the quasiperiodic nature of the spectrum.
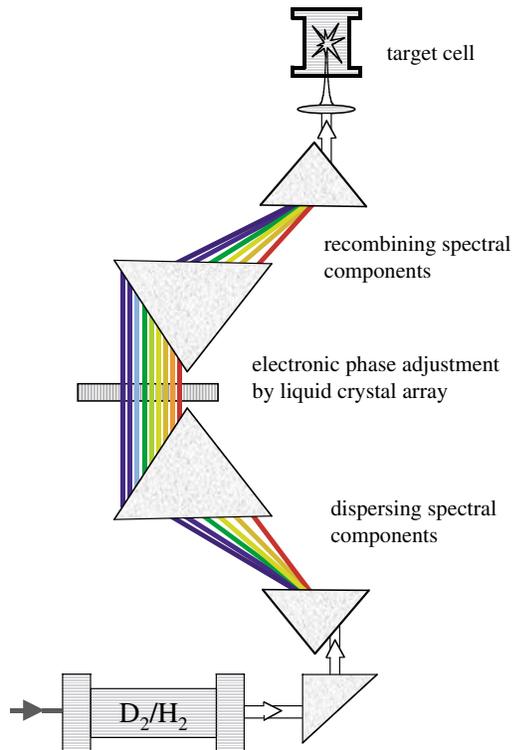
FIG. 3 (color online). Experimental setup for the temporal correlation experiment. The spectrum is spatially separated with a prism pair, which allows independent phase control of individual sidebands with the liquid crystal array. Because of the limitations of the liquid crystal, we use 15 visible sidebands extending in wavelength from 650 to 420 nm. The sidebands are spatially recombined with another prism pair and focused into an NO ionization chamber.

and NO^+ ions are detected with a Channeltron electron multiplier. The dissociation of NO molecules is negligible.

When all 15 sidebands are present and making comparable contributions to the ion signal, our calculations predict that varying the phase of one sideband at a time will result in a roughly sinusoidal change in the ion signal. In Fig. 4, plots (a) and (b) show two examples of these interferences. The solid circles in each of these plots are the experimental data points obtained by averaging over 200 shots, and the solid line is the sinusoidal fit to the data. In plot (c), three vibrational sidebands are present (650, 540, and 468 nm) and the phase of the red sideband is changed. In plot (d) two rovibrational sidebands at the red end (650 and 626 nm) and two at the violet end (420 and 430 nm) of the spectrum are present. In all of these plots we observe a sinusoidal change of the ion signal with good contrast. In particular, plot (d) proves the mutual coherence between the ends of the spectrum.

The 15 coherent sidebands used in our experiment are predicted to form a train of pulses with 3-fs pulse width, separated by 57 fs. To test this prediction, we performed a cross-correlation measurement. Initially, we optimize sideband phases to give the maximum ion signal, thereby
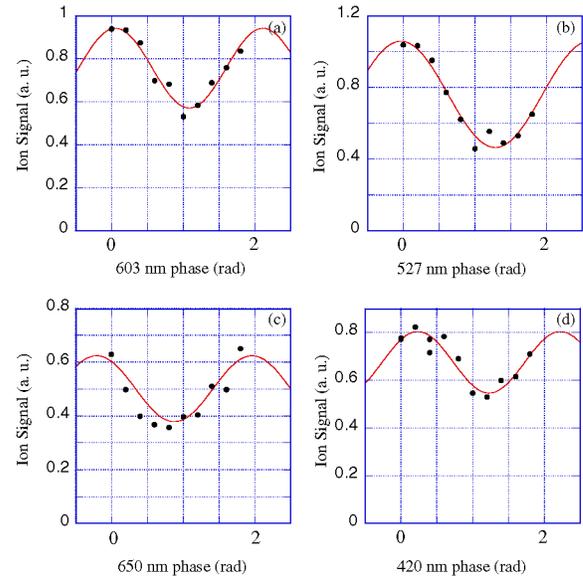
FIG. 4 (color online). The ion signal as a function of the phase of a single sideband. In plots (a) and (b) all fifteen sidebands are present. In plot (c) three vibrational sidebands (650, 540, and 468 nm) are present, whereas, in plot (d), two rovibrational sidebands at the red end (650 and 626 nm) and two at the violet end (420 and 430 nm) of the spectrum are present.

synthesizing a single pulse. Then, starting from 650 nm and going to 420 nm, we add to every other sideband a phase proportional to its frequency, effectively time delaying those sidebands. This corresponds to synthesizing two pulses, one of which is delayed with respect to the other. By varying this time delay and measuring the ion signal, we obtain a cross correlation, shown in Fig. 5 by the solid circles. Such a cross-correlation trace is predicted to have almost the same width as the actual time waveform. Because of the nonlinearity of multiphoton ionization, most ions are produced by the peak of the ns-long sideband envelopes. We therefore model the field as a sum of monochromatic waves:

$$E(t) = \sum_{\substack{\text{odd} \\ \text{sidebands}}} E_{q,r}\cos[\omega_{q,r}(t+\tau)] + \sum_{\substack{\text{even} \\ \text{sidebands}}} E_{q,r}\cos(\omega_{q,r}t),$$

(4)

where the field strengths $E_{q,r}$ are determined from measurements of sideband energies. We treat NO molecules as fourth-order detectors and calculate the ion signal as $\int E^8(t)dt$. This time-domain calculation of the correlation trace is shown as the dashed line in Fig. 5. We observe good agreement between experiment and theory. The experimental trace has a longer pulse width (≈ 5 fs) which is probably due to an imperfect overlap of the sidebands at the focus.

Because of the low damage threshold of the liquid crystal, we cannot focus each sideband to a single pixel on the liquid-crystal modulator. Each sideband goes through a number of pixels, and phase delay is achieved by applying the same voltage to each of the pixels. We
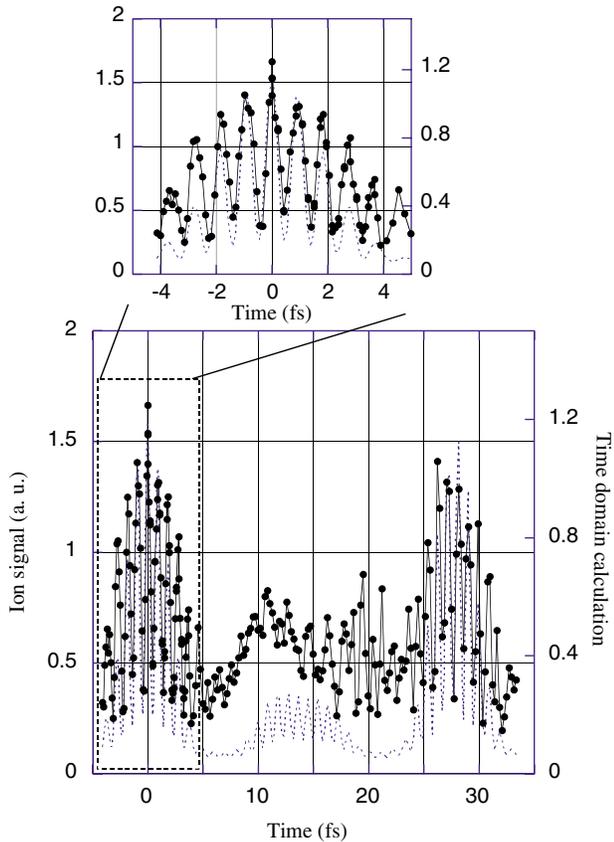
FIG. 5 (color online). The ion signal as a function of time delay between two pulses (electronically) synthesized by two sets of sidebands. The time delay is achieved electronically by applying a specified phase to each sideband. The solid circles are the data points and the solid line connects these points. The dashed line is the time-domain calculation.

observe an unexplained change in the focal spot size when we change the phase of each sideband [19]. This change in spot size limits our resolution of the ion signal to $\pm 15\%$ in Fig. 5. We have experimentally confirmed that this effect does not change the shape or the structure of the cross-correlation waveform.

In summary, we have demonstrated a new quasiperiodic Raman technique that shows promise for generation of subfemtosecond pulses in the optical region. We have shown mutual coherence among 15 sidebands in a wide spectrum covering the infrared, visible, and ultraviolet regions. We have not observed any reduction in the contrast of the interference fringes as the number of sidebands increases. If phase control can be extended over the full spectrum, it will be possible to synthesize arbitrary waveforms with pulse widths less than 1 fs.

[1] S. E. Harris and A. V. Sokolov, Phys. Rev. Lett. **81**, 2894 (1998); A. V. Sokolov, D. R. Walker, D. D. Yavuz, G. Y. Yin, and S. E. Harris, Phys. Rev. Lett. **85**, 562 (2000); D. D. Yavuz, D. R. Walker, G. Y. Yin, and S. E. Harris, Opt. Lett. **27**, 769 (2002).

[2] J. Q. Liang, M. Katsuragawa, F. Le Kien, and K. Hakuta, Phys. Rev. Lett. **85**, 2474 (2000); M. Katsuragawa, J. Q. Liang, F. Le Kien, and K. Hakuta, Phys. Rev. A **65**, 025801 (2002).

[3] A. V. Sokolov, D. R. Walker, D. D. Yavuz, G. Y. Yin, and S. E. Harris, Phys. Rev. Lett. **87**, 033402 (2001).

[4] S. E. Harris, D. R. Walker, and D. D. Yavuz, Phys. Rev. A **65**, 021801(R) (2002).

[5] H. Bohr, *Almost Periodic Functions* (Chelsea Publishing, New York, 1947).

[6] S. Yoshikawa and T. Imasaka, Opt. Commun. **96**, 94 (1993).

[7] A. E. Kaplan, Phys. Rev. Lett. **73**, 1243 (1994); A. E. Kaplan and P. L. Shkolnikov, J. Opt. Soc. Am. B **13**, 347 (1996).

[8] A. Nazarkin, G. Korn, M. Wittmann, and T. Elsaesser, Phys. Rev. Lett. **83**, 2560 (1999); M. Wittmann, A. Nazarkin, and G. Korn, Phys. Rev. Lett. **84**, 5508 (2000); M. Wittmann, A. Nazarkin, and G. Korn, Opt. Lett. **26**, 298 (2001); N. Zhavoronkov and G. Korn, Phys. Rev. Lett. **88**, 203901 (2002).

[9] L. L. Losev and A. P. Lutsenko, Quantum Electron. **23**, 919 (1993); G. S. McDonald, G. H. C. New, L. L. Losev, A. P. Lutsenko, and M. Shaw, Opt. Lett. **19**, 1400 (1994).

[10] H. Kawano, Y. Hirakawa, and T. Imasaka, Appl. Phys. B **65**, 1 (1996); IEEE J. Quantum Electron. **34**, 260 (1998).

[11] S. Uetake, R. S. D. Sihombing, and K. Hakuta, Opt. Lett. **27**, 421 (2002); S. Uetake, M. Katsuragawa, M. Suzuki, and K. Hakuta, Phys. Rev. A **61**, 011803(R) (1999).

[12] R. A. Bartels, T. C. Weinacht, N. Wagner, M. Baertschy, C. H. Greene, M. M. Murnane, and H. C. Kapteyn, Phys. Rev. Lett. **88**, 013903 (2002).

[13] P. M. Paul *et al.*, Science **292**, 1689 (2001); M. Hentschel *et al.*, Nature (London) **414**, 509 (2001); A. Baltuska *et al.* Nature (London) **421**, 611 (2003).

[14] A. Baltuska *et al.*, Opt. Lett. **22**, 102 (1997); A. Baltuska *et al.*, Opt. Lett. **27**, 306 (2002).

[15] A. Assion, T. Baumert, J. Helbing, V. Seyfried, and G. Gerber, Chem. Phys. Lett. **259**, 488 (1996); T. Baumert, T. Brixner, V. Seyfried, M. Strehle, and G. Gerber, Appl. Phys. B **65**, 779 (1997).

[16] B. J. Pearson, J. L. White, T. C. Weinacht, and P. H. Bucksbaum, Phys. Rev. A **63**, 063412 (2001).

[17] R. A. Bartels, T. C. Weinacht, S. R. Leone, H. C. Kapteyn, and M. M. Murnane, Phys. Rev. Lett. **88**, 033001 (2002).

[18] A. V. Sokolov, D. D. Yavuz, and S. E. Harris, Opt. Lett. **24**, 557 (1999).

[19] This effect may be due to two reasons: (i) The two glass surfaces that contain the liquid-crystal form a weak Fabry-Perot etalon. When a voltage is applied, the resonant frequency of the etalon changes and causes a slight change in the transmission of the sideband. (ii) Because of the 3-μm gap between adjacent pixels, each sideband goes through a phase grating. The depth of the grating changes as a function of the applied voltage and causes the sideband to focus slightly differently.